REPORT SAMSO-TR-76-209

(12)

Evaluation of Nonisothermal Band Models for H_2O

Chemistry and Physics Laboratory
Laboratory Operations
The Aerospace Corporation
El Segundo, Calif. 90245

1 October 1976

Interim Report

APPROVED FOR PUBLIC RELEASE;
DISTRIBUTION UNLIMITED

Sponsored by
DEFENSE ADVANCED RESEARCH PROJECTS AGENCY (DoD)
Monitored by SAMSO Under Contract No. F04701-76-C-0077

DARPA Order No. 2843

SPACE AND MISSILE SYSTEMS ORGANIZATION
AIR FORCE SYSTEMS COMMAND
Los Angeles Air Force Station
P.O. Box 92960, Worldway Postal Center
Los Angeles, Calif. 90009

This report was submitted by The Aerospace Corporation, El Segundo, CA 90245, under Contract No. F04701-76-C-0077 with the Space and Missile Systems Organization (SAMSO), Deputy for Advanced Space Programs, P.O. Box 92960, Worldway Postal Center, Los Angeles, CA 90009. It was reviewed and approved for The Aerospace Corporation by A. H. Silver, Director, Electronics Research Laboratory. Lieutenant Colonel John R. Doughty, SAMSO/YAD, was the project officer. This research was supported by the Defense Advanced Research Projects Agency of the Department of Defense.

This report has been reviewed by the Information Office (OI) and is releasable to the National Technical Information Service (NTIS). At NTIS, it will be available to the general public, including foreign nations.

This technical report has been reviewed and is approved for publication. Publication of this report does not constitute Air Force approval of the report's findings or conclusions. It is published only for the exchange and stimulation of ideas.

FOR THE COMMANDER

John R Doughty Lt Col, USAF

John R. Doughty, Lt Col, USAF
Manager, HEL Technology Function
Development Directorate

UNCLASSIFIED

SECURITY CLASSIFICATION OF THIS PAGE (When Data Entered)

REPORT DOCUMENTATION PAGE

READ INSTRUCTIONS BEFORE COMPLETING FORM

19

1. REPORT NUMBER

18 SAMSO-TR-76-209

2. GOVT ACCESSION NO.

3. RECIPIENT'S CATALOG NUMBER

4. TITLE (and Subtitle)

6 EVALUATION OF NONISOTHERMAL BAND MODELS FOR H_2O.

5. TYPE OF REPORT & PERIOD COVERED

9 Interim rept.

6. PERFORMING ORG. REPORT NUMBER

14 TR-0077(2753-04)-2

7. AUTHOR(s)

10 Stephen A. Young

8. CONTRACT OR GRANT NUMBER(s)

15 F04701-76-C-0077, new

9. PERFORMING ORGANIZATION NAME AND ADDRESS

The Aerospace Corporation
El Segundo, Calif. 90245

10. PROGRAM ELEMENT, PROJECT, TASK AREA & WORK UNIT NUMBERS

ARPA Order-2843

11. CONTROLLING OFFICE NAME AND ADDRESS

Defense Advanced Research Projects Agency
Arlington, Va. 22209

12. REPORT DATE

11 1 Oct[illegible]r [illegible]76

13. NUMBER OF PAGES

45

14. MONITORING AGENCY NAME & ADDRESS (if different from Controlling Office)

Space and Missile Systems Organization
Air Force Systems Command
Los Angeles, Calif. 90009

12 46p.

15. SECURITY CLASS. (of this report)

Unclassified

15a. DECLASSIFICATION/DOWNGRADING SCHEDULE

16. DISTRIBUTION STATEMENT (of this Report)

Approved for public release; distribution unlimited

17. DISTRIBUTION STATEMENT (of the abstract entered in Block 20, if different from Report)

18. SUPPLEMENTARY NOTES

19. KEY WORDS (Continue on reverse side if necessary and identify by block number)

High-temperature H_2O spectra

H_2O band model parameters

20. ABSTRACT (Continue on reverse side if necessary and identify by block number)

Comparisons of predicted and measured radiance spectra for nonuniform hot H_2O gas samples are reported. The predicted spectra are generated with band models formulated in a companion paper, and band model parameters constructed to handle optical path temperature variations from 200 to 3000°K. The model identified in the companion paper as the intuitive derivative approximation is shown to be superior to the traditional Curtis-Godson approximation in treating general optical paths along which high degrees of nonuniformity occur.

DD FORM 1473 (FACSIMILE)

409383

UNCLASSIFIED

SECURITY CLASSIFICATION OF THIS PAGE (When Data Entered)

YB

CONTENTS

TABLE

FIGURES

FIGURES (Continued)

I. INTRODUCTION

In a companion paper,* eight models for computing the spectral radiance of nonuniform optical paths are considered theoretically. All of the models are formulated within the statistical band model but differ in the manner in which inhomogeneity and nonisothermality of the path are treated. In this paper, predictions of these models are compared with experimental measurements on H_2O in the 2.7-μm spectral region. Application of the models requires band model parameters for the 2.7-μm water band and for the range of temperatures that occur along the optical paths considered. Construction of a set of parameters suitable for use in the 200 to 3000°K temperature range is considered in Section II.

Radiance and transmittance measurements on nonuniform H_2O samples that are suitable for quantitative comparison with theoretical prediction have been made by several groups.(1-7) Radiance comparisons are made here with results of Refs. 3, 5, and 7 and are discussed in Section III. The conclusion drawn from these and other unreported comparisons is that when the various models predict different results, the model identified in the companion paper as the intuitive derivative approximation yields the best agreement with experiment. Only the results for this approximation and Godson's version of the Curtis-Godson (CG) approximation (see companion paper) are presented.

---

*Stephen Young, "Nonisothermal Band Model Theory," J. Quantum Spectroscoy Radiative Transfer (to be published).

II. BAND MODEL PARAMETERS

A. NASA (GENERAL DYNAMICS) PARAMETERS

H_2O band model parameters used in this work were constructed[8] by combining the high-temperature NASA parameters[3] with low-temperature parameters derived from the AFGL atmospheric absorption line data compilation.[9] The NASA parameters are tabulated through the 2.7-μm band in 25 cm^{-1} increments and for a spectral resolution $\Delta\nu \simeq 25\ cm^{-1}$. The absorption parameter $\bar{k}$ is given in the temperature range 300 to 3000°K, but the $\bar{\delta}$ parameter for only 600 to 3000°K. (For low-temperature application of these parameters, $\bar{\delta}$ is extrapolated semilogarithmically from the 600 and 1000°K tabulated data.) Above ~ 1200°K, the NASA parameters were obtained in a consistent manner from emission-absorption measurements made on long strip-burner H_2/O_2 flames.[10] Data below ~ 1200°K are based on extrapolations from these high-temperature data and on analysis of published low-temperature H_2O spectra. The unit of $\bar{k}$ in the NASA tabulation is cm^{-1} at standard temperature and pressure and has to be multiplied by 273/T to obtain $\bar{k}$ with the natural unit cm^{-1}/atm. The unit of $\bar{\delta}$ is cm^{-1}.

The line width band model parameter for the NASA parameters is given by

$$\bar{\gamma}(p, T) = p\left[c_{H_2O}\bar{\gamma}^*\left(\frac{273}{T}\right)^{n^*} + \sum_f c_f\bar{\gamma}_f\left(\frac{273}{T}\right)^{n_f}\right] \tag{1}$$

The summation term represents foreign-gas broadening ($f \neq H_2O$) and nonresonant self-broadening ($f = H_2O$) contributions to the line width. The first term accounts for resonant self-broadening effects. The c factors are the mole fraction concentrations of the gas constituents, and the $\overline{\gamma}$ factors are broadening parameters for standard temperature (273°K) and pressure (1 atm) conditions. The exponential factors n determine the degree of temperature variation for the various broadening mechanisms. Values of n and $\overline{\gamma}$ are given in Table I. The present work involves only N_2 and O_2 as foreign gas broadeners.

Although quite adequate for $T > 1200°K$, the NASA parameters are not particularly useful for application near room temperature. This inadequacy is demonstrated in Figs. 1 and 2, where the predicted* transmittance spectra of two uniform gas samples at 296°K are compared with experimental spectra.[11] The NASA parameters seriously underestimate the degree of absorption. Since this discrepancy is evident even for weak absorption, it is not caused solely by errors in the extrapolation used to get $\overline{\delta}$. A 1040°K emission spectrum generated with these parameters is compared with an experimental spectrum[12] in Fig. 3(a). Here, the agreement is adequate, although not as good as is obtained for $T > 1200°K$. A slight underprediction

*All band model calculations in this section are made with the uniform path statistical model with exponential-tailed inverse line strength distribution.

Table I. Line-Broadening Parameters for H_2O[†]

Broadener	$\bar{\gamma}^*$ (cm^{-1}/atm)	n^*	$\bar{\gamma}_f$ (cm^{-1}/atm)	n_f
H_2O	0.44	1.0	(0.09)	0.5
N_2			0.09	0.5
O_2			0.04	0.5

[†]Data taken from Reference 3. Value in parentheses is estimated.

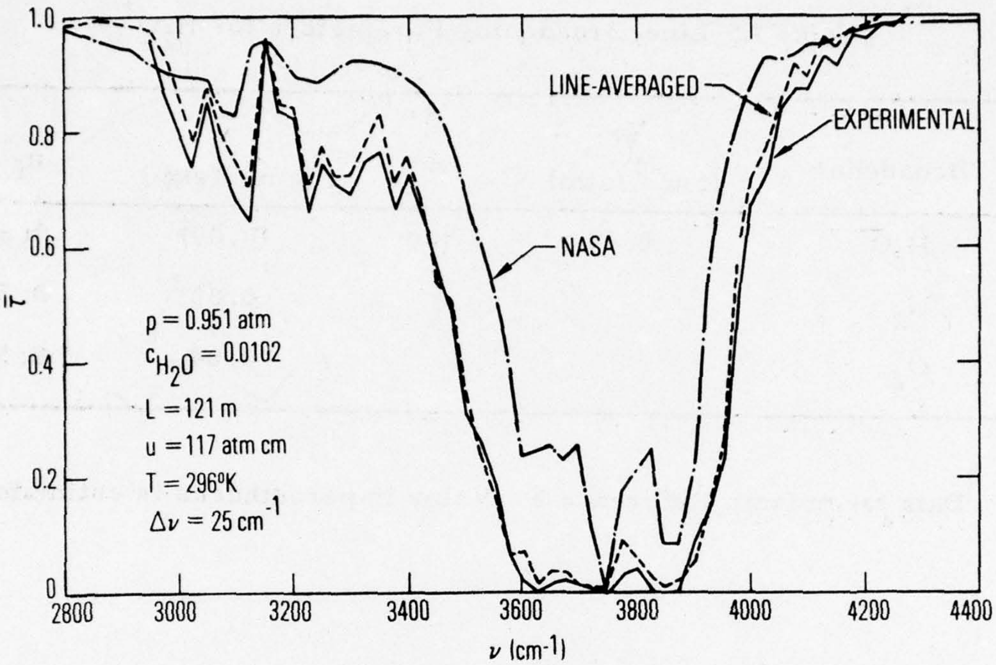

Fig. 1. Low-Temperature Transmittance Spectra for H_2O. ———————— experimental curve derived from the tables of Ref. 11 for sample No. 39 and $\Delta\nu$ = 25 cm^{-1}; ——— · ——— · ——— band model prediction with NASA parameters; — — — — — — band model prediction with line-average or combined parameters.

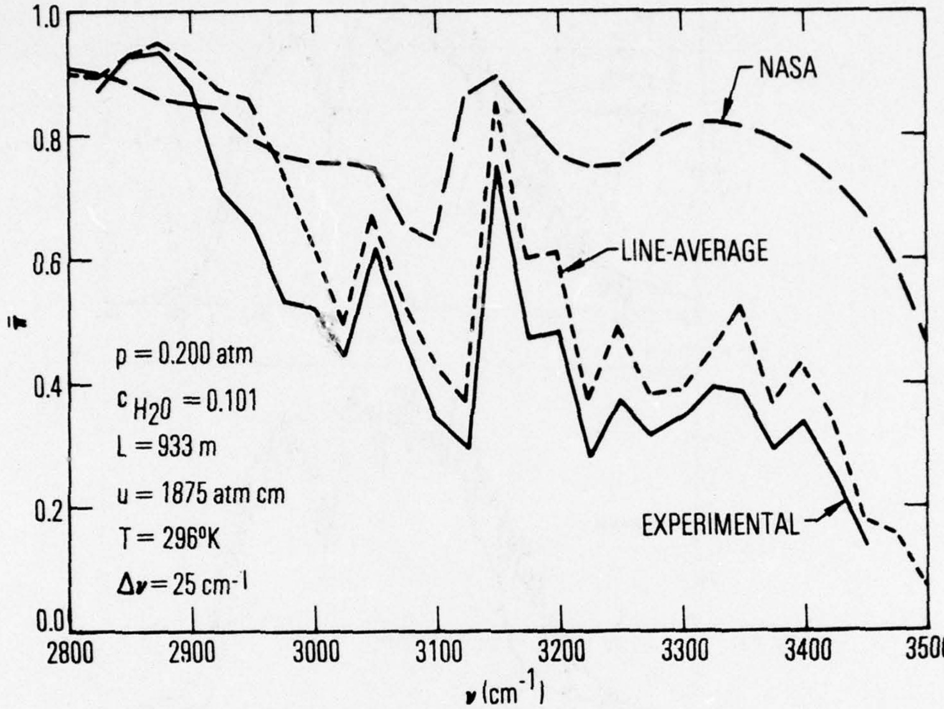

Fig. 2. Low-Temperature Transmittance Spectra for H_2O in the Band Wing Regions. ———— experimental curve derived from the tables of Ref. 11 for sample No. 40 and $\Delta\nu$ = 25 cm^{-1}; — — — — — — — band model prediction with NASA parameters; - - - - - - band model prediction with line-average or combined parameters.

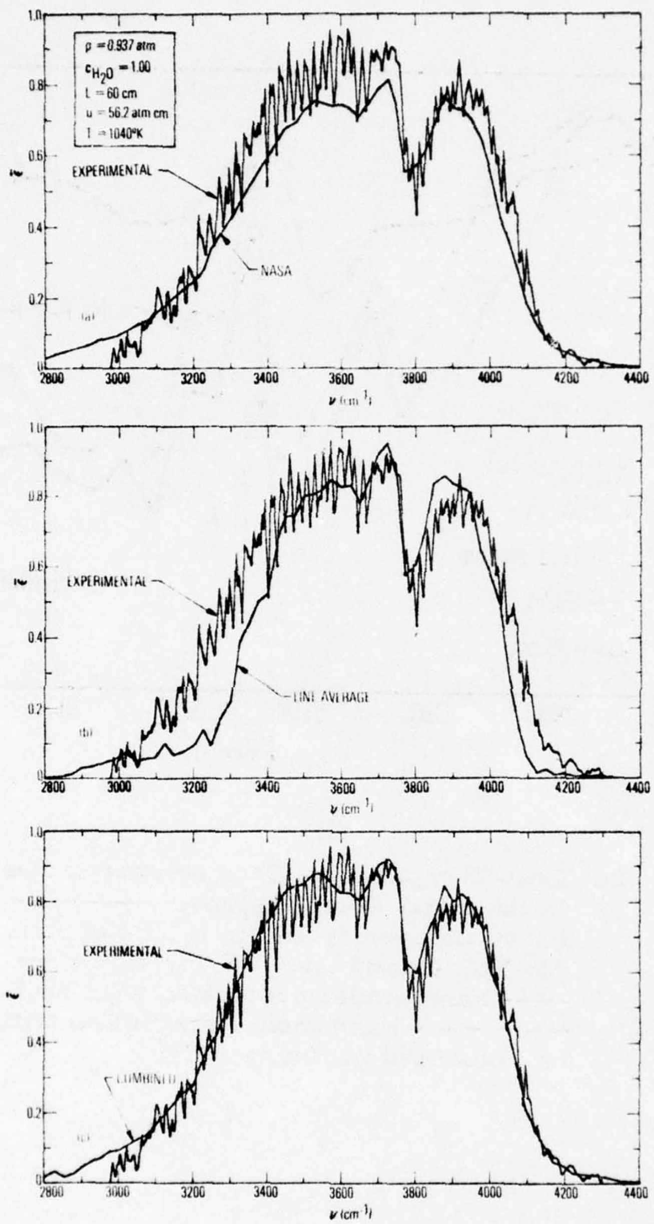

Fig. 3. High-Temperature Emission Spectra for H_2O. The jagged curve is an experimental spectrum from Ref. 12. The smooth curves are band model results predicted with the indicated band model parameter set.

of emissivity is evident throughout the band. Other comparisons of experimental hot H_2O radiance and transmittance spectra with predictions using the NASA parameters have been made in Refs. 3, 8, and 13.

B. LINE-AVERAGED PARAMETERS

Band-model parameters were constructed from the AFGL line data compilation according to the line averaging procedure described in Section III. D of the companion paper. The data given for each line in this compilation are the line position $\nu(\mathrm{cm}^{-1})$, the line strength S_a (cm^{-1}/molecule-cm^{-2} at $T_a = 296°\mathrm{K}$), the line half-width γ_a (cm^{-1} for air-broadening at 296°K and 1 atm pressure), and the energy of the lower level of the transition E (cm^{-1}). The temperature dependence of line strength for the $i^{\underline{th}}$ line was taken as

$$S(i,T) = C(T)\, S_a(i) \frac{Q_R(T_a)\, Q_V(T_a)}{Q_R(T)\, Q_V(T)} \left[\frac{1 - e^{-\nu(i)/kT}}{1 - e^{-\nu(i)/kT_a}}\right] \times \exp\left[-\frac{E(i)}{k}\left(\frac{1}{T} - \frac{1}{T_a}\right)\right]. \tag{2}$$

Q_R and Q_v are, respectively, the rotational and vibrational partition functions of the molecule. The ratio of rotational partition functions was approximated by

$$\frac{Q_R(T_a)}{Q_R(T)} \simeq \left(\frac{T_a}{T}\right)^m \tag{3}$$

with m = 1.5. The vibration partition function was assumed to be the product of simple harmonic oscillator partition functions for each vibrational mode j of the molecule

$$Q_V(T) = \prod_{j=1}^{3} \left[1 - e^{-\nu_j/kT}\right]^{-d_j} \tag{4}$$

where ν_j are the fundamental oscillatory frequencies of the molecule and d_j are the degeneracies of these modes. For H_2O, $\nu_1 = 3657.0$, $\nu_2 = 1594.7$, $\nu_3 = 3755.7\ cm^{-1}$, and all d_j are unity. The exponential term of equation (2) accounts for the Boltzmann distribution population of molecules, and the term in brackets accounts for stimulated emission. k is Boltzmann's constant; $1/k = 1.439$ cm-°K. The factor C(T) of equation (2) converts the line strength from the AFGL unit cm^{-1}/molecule $-cm^{-2}$ to the unit cm^{-2}/atm and is

$$C(T) = 2.480 \times 10^{19} \frac{296°K}{T} \qquad (\text{molecules/atm-cm}^3) \tag{5}$$

Equations (2) through (5) give the required line strength S(i, T) to be used in equation (35) of the companion paper to calculate the absorption parameter $\overline{k}$ with unit cm^{-1}/atm for any desired spectral interval $\Delta\nu$ and temperature T.

A mean value of $\gamma_a(i)$ was made directly from the AFGL data. This mean value $\overline{\gamma}_a$ was used with $\gamma_a(i)$ and S(i, T) to compute $\overline{\delta}$ by equations (36) and (37) of the companion paper. The line-broadening model of equation (1) was used for this formulation of line-averaged parameters. Transformation

of $\bar{\gamma}_a$ from the AFGL conditions of air-broadening at 296°K to the conditions of resonant self-, nonresonant self-, and foreign-gas broadening at 273°K were made using the data of Table I and an assumed air composition c_{N_2} = 0.78, c_{O_2} = 0.22. The transformations are:

$$\bar{\gamma}^* = 5.800\ \bar{\gamma}_a$$
$$\bar{\gamma}_{H_2O} = 1.186\ \bar{\gamma}_a$$
$$\bar{\gamma}_{N_2} = 1.186\ \bar{\gamma}_a$$
$$\bar{\gamma}_{O_2} = 0.527\ \bar{\gamma}_a$$

The AFGL data compilation was constructed specifically for application to atmospheric problems, and it would be expected that band model parameters derived from this data would be suitable for low-temperature applications. This expectation is substantiated in Figs. 1 and 2, where spectra computed with the line-averaged parameters are compared with experimental transmittance spectra. On the other hand, the AFGL compilation does not include many lines that originate from high vibrational and rotational levels. Since these lines are important at high temperatures, it is expected that the line-averaged parameters will fail at high temperatures. This failure at 1040°K is demonstrated in Fig. 3(b), where it is evident that a serious underprediction of emissivity is made for the band wings.

C. COMBINED PARAMETERS

Neither the NASA parameters nor the line-averaged parameter themselves are suitable for use in problems involving optical paths along

which the temperature may vary from atmospheric to gas combustion values. The NASA parameters are adequate at the higher temperatures, and the line-averaged parameters are adequate at the lower temperatures. For the reverse situation, each parameter set fails. A parameter set that is consistent for the whole temperature range from ~ 200 to $\sim 3000°K$ was generated by combining these two parameter sets. This combination was performed for each 25 cm^{-1} interval between 2500 and 4500 cm^{-1} by making semilogarithmic plots of the parameters $\overline{k}$ and $\overline{\delta}$ from each set as a function of temperature and drawing a smooth transition curve from one set to the other. A detailed discussion of this method is given in Ref. 8. Two examples are given in Figs. 4 and 5. The variation of the line-averaged parameter $\overline{k}$ at 2500 cm^{-1} shown in Fig. 4 is typical for all of the spectral intervals in the band wings. The absorption coefficient increases with temperature up to $\sim 1000°K$ but thereafter levels-off or falls slightly due to lack of "hot line" data in the AFGL compilation. This example at 2500 cm^{-1} is also a case of extreme transition between the two component parameter sets. In general, throughout regions of strong absorption (e.g., ν = 3700 cm^{-1}, Fig. 5) the match-up procedure was relatively self-evident. The final combined parameter set generated is tabulated in the Appendix. Low-temperature transmittance spectra generated with the combined parameters are indistinguishable from the spectra of Figs. 1 and 2 generated with the line-averaged parameters. The 1040°K emission spectrum computed with the combined parameters is shown in Fig. 3(c), where it can be seen that the agreement with experiment

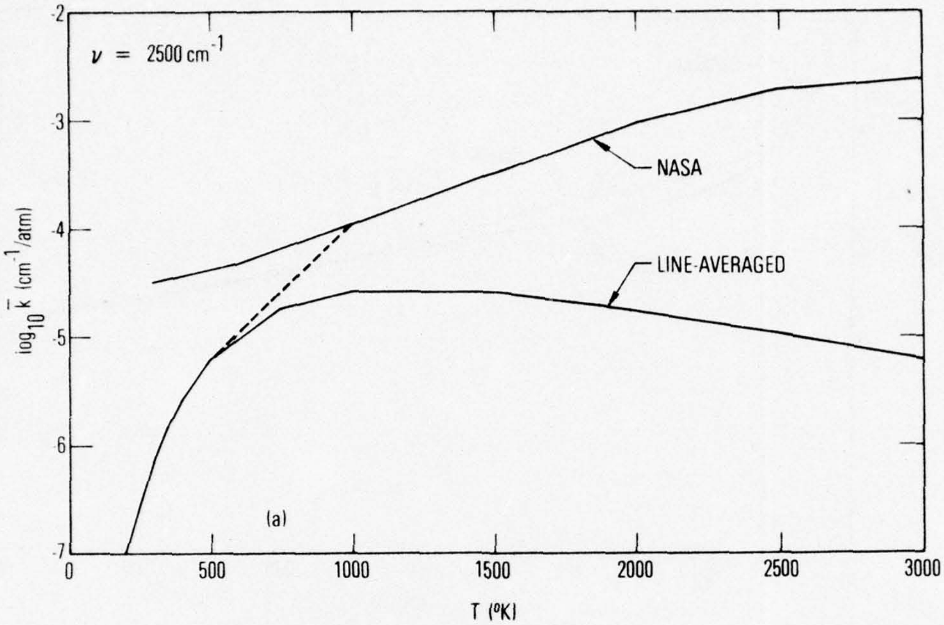

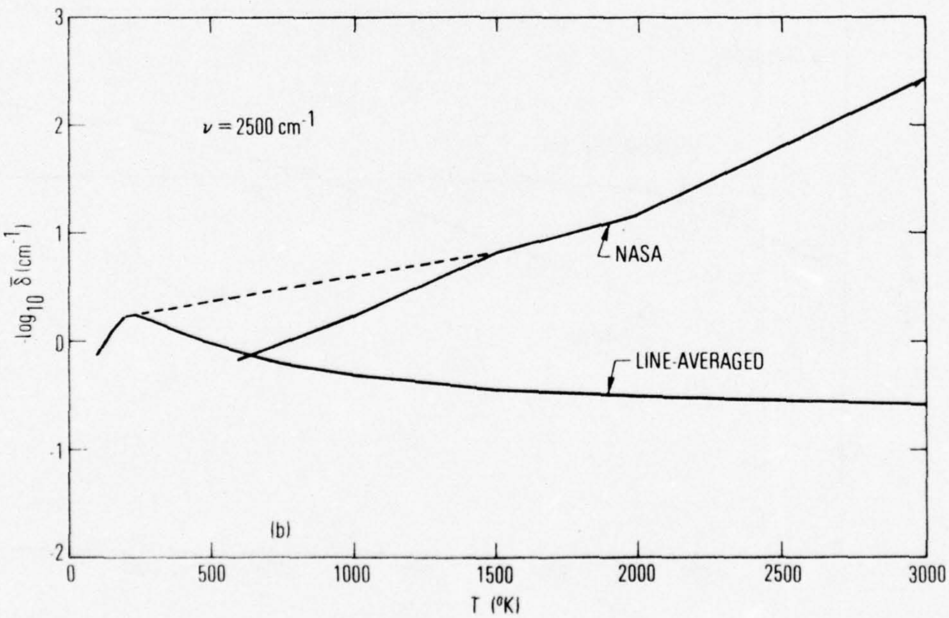

Fig. 4. Parameter Match-Up at $\nu = 2500\ cm^{-1}$. The dashed line indicates the assumed transition from the NASA to line-averaged parameter curve.

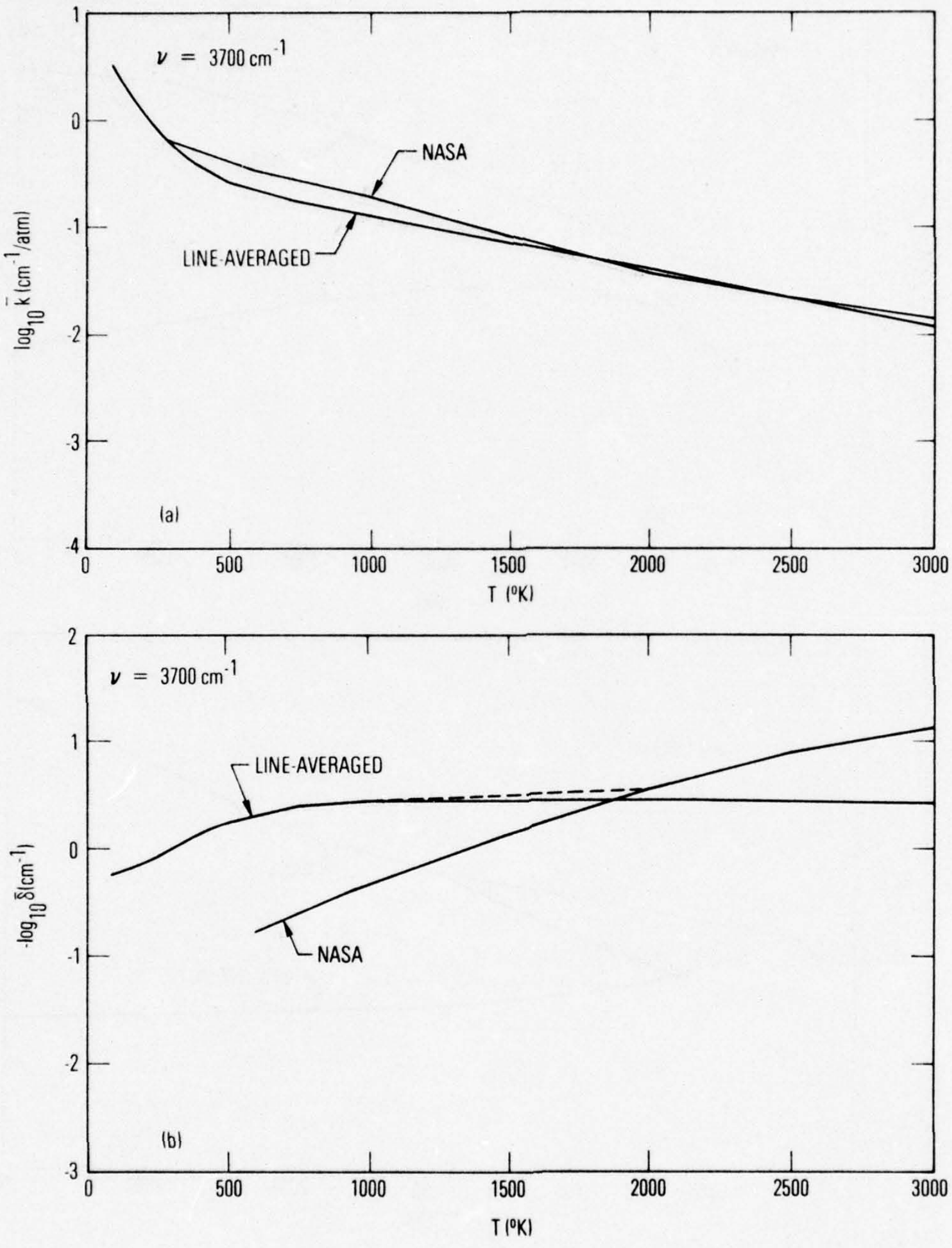

Fig. 5. Parameter Match-Up at ν = 3700 cm^{-1}

is better than is obtained with either of the component parameter sets. Above 1200° K, the combined parameters reproduce spectra obtained with the NASA parameters. The combined parameters are used exclusively in computing the spectra of Section III.

D. DISCUSSION

A theoretical result of the companion paper was that if the distribution of line strengths in a spectral interval $\Delta\nu$ is described by an inverse strength function, the line density function $1/\delta$ should be a linear function of temperature. Linear plots of $1/\delta$ vs T from the NASA, line-averaged, and combined parameters for the 25-cm^{-1} interval centered at 3700 cm^{-1} are shown in Fig. 6. Clearly, none of the sets displays a realistic linear temperature variation. The line-averaged parameters display the characteristic saturation feature caused by the lack of hot-line data in the AFGL compliation. The NASA parameters appear to obey a power law in temperature. The long-dashed line is a linear variation suggested by the nearly linear portion of the line-averaged parameter plot between 200 and 700°K. Compared to this line, $1/\delta$ from the combined parameter set displays the most nearly linear variation, although deviations from linearily are substantial. The construction of the combined parameter set was made prior to the discovery (at least by this author) of this predicted linearity, and possibly a better combining procedure could have been made with this result as a contributing construction criterion. With the known success of the inverse line strength distribution in treating water by band model methods

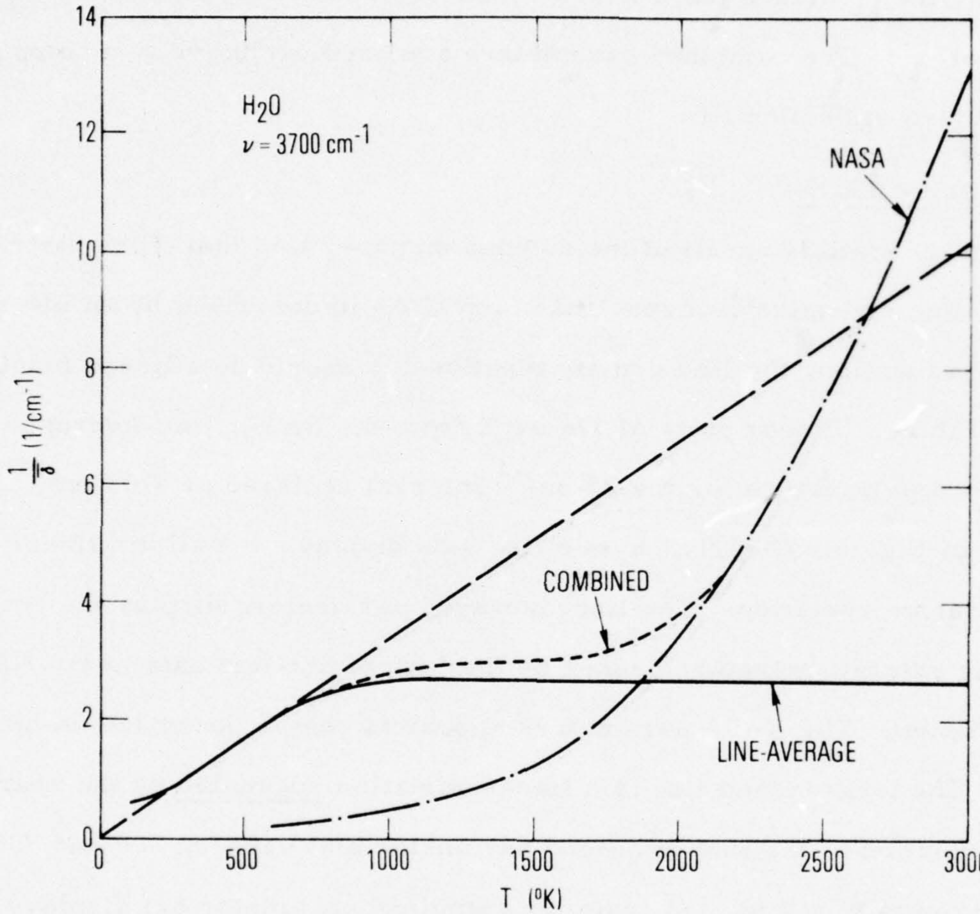

Fig. 6. Temperature Variation of $1/\delta$ at ν = 3700 cm^{-1}

considered, the conclusion that the results of Fig. 6 invalidate this distribution should not be made hastely. Rather, more investigation (both theoretical and experimental) should be made on the "temperature-consistency" of band-model parameters. For example, a significant assumption that has been made in combining the NASA and line-averaged parameter sets is that the parameters $\overline{k}$ and $\overline{\delta}$ from each set represent the same quantity. Only within the confines of the modelling assumptions is this true. In fitting the models to experimental data, two entirely different approaches are used to define these parameters, one based on detailed line measurements and one based on low-resolution emission-absorption measurements.

III. TEST CASES AND RESULTS

A. NONISOTHERMAL EMISSION CELL MEASUREMENTS

The nonisothermal hot-gas radiance studies of Simmons et al.[5] include two measurements for H_2O. The measurements were made on pure H_2O confined to a 60-cm emission cell along which a thermal gradient could be maintained. Temperature profiles for the two cases are shown in Fig. 7. Both samples were homogeneous (no pressure or concentration gradients) with c = 1 and p = 1.0 atm (Case 1), p = 0.91 atm (Case 2). Experimental radiance spectra are shown in Figs. 8 and 9.

Calculations were performed by dividing the optical path into N = 20 equal length intervals and interpolating for the pressure, temperature, and H_2O concentration at the 21 points defining the path. These data were then used to compute and interpolate for the band model parameters $\overline{k}$, $\overline{\delta}$, and $\overline{\gamma}$ at each point along the path. Once these six quantities were defined along the path, the various band models were applied. Path integrals used to define averaged band model parameters and to compute radiance were performed by trapezoidal quadrature. The selection of 20 intervals was made on the basis of the following: The largest value of $\overline{k}$ occurring in the spectral and temperature range considered is $\overline{k} \simeq 0.8\ cm^{-1}/atm$ and occurs at $\nu \sim 3750\ cm^{-1}$, $T \sim 400°K$. The characteristic absorption length for this condition is $L_a = (cp\overline{k})^{-1} \simeq 1.3$ cm. In order for the numerical integration to be accurate, the integration interval should be less than this value. With

PRECEDING PAGE BLANK-NOT FILMED

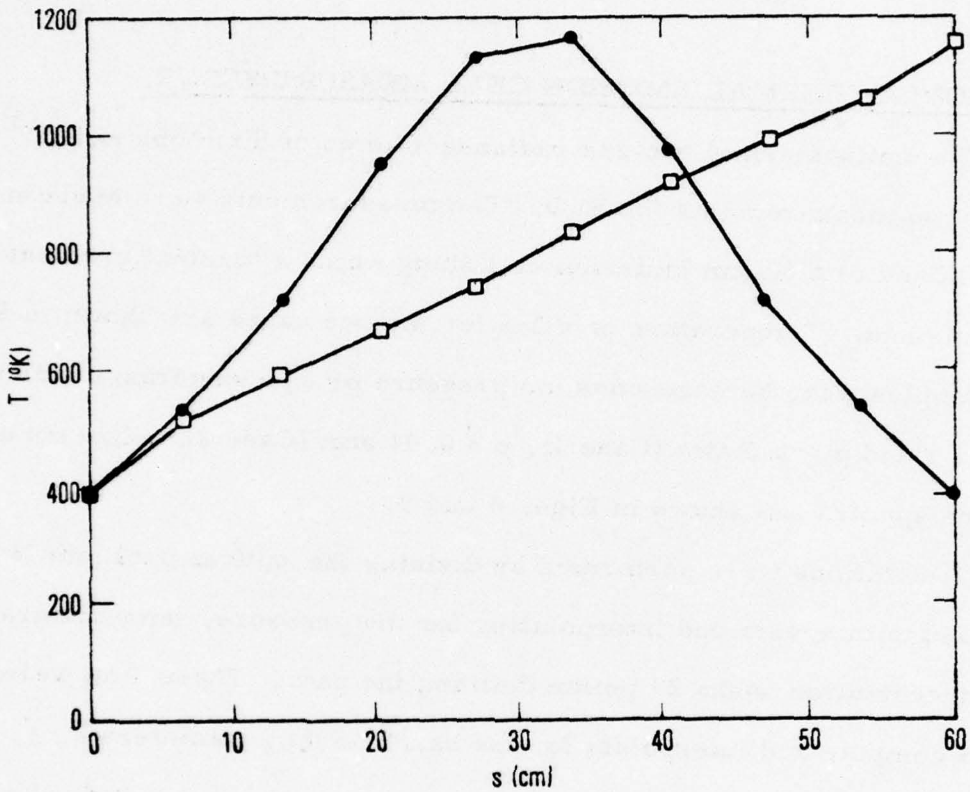

Fig. 7. Temperature Profiles for Nonisothermal Emission Cell Measurements. —●— Case 1(Run 10216811 of Ref. 5), T = 382, 537, 723, 953, 1128, 1160, 990, 751, 558, 389° K; —□— Case 2 (Run 10246813 of Ref. 5), T = 392, 513, 593, 671, 745, 835, 918, 993, 1059, 1152° K.

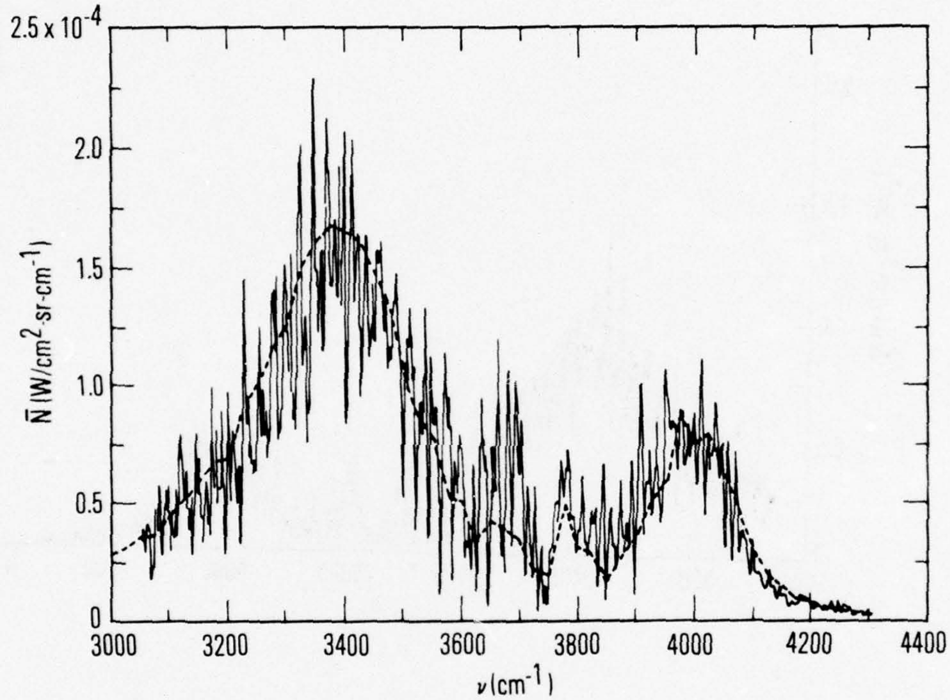

Fig. 8. Radiance Spectra for Case 1 of Nonisothermal Emission Cell Study

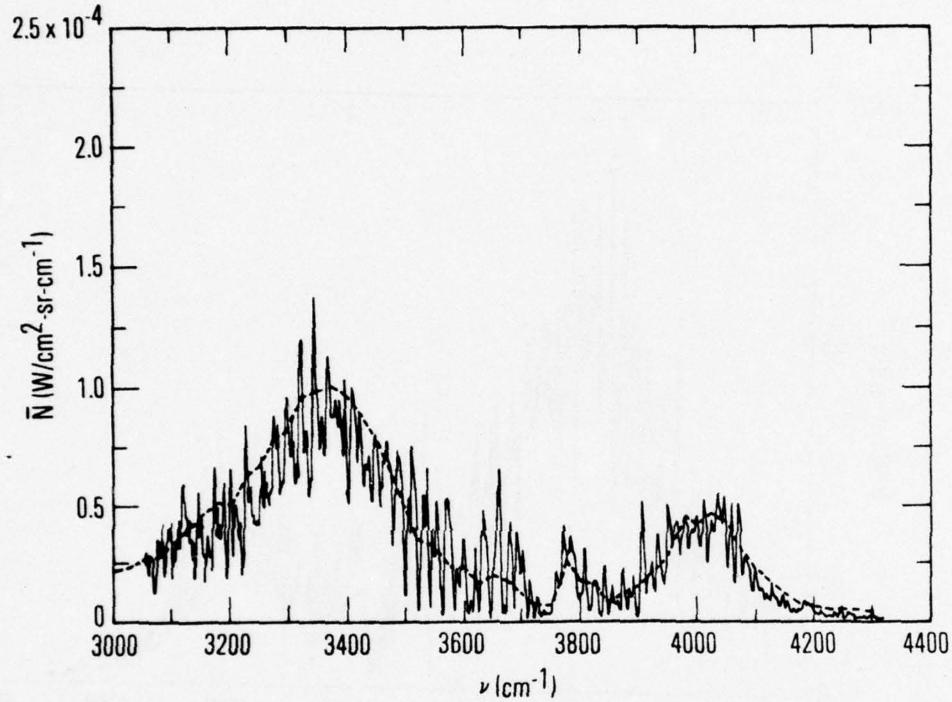

Fig. 9. Radiance Spectra for Case 2 of Nonisothermal Emission Cell Study

a total path length of 60 cm, N should be greater than ~ 40. This is a worst-case estimate, however, and N = 20 was found to be adequate.

For both cases, all models predicted the same radiance spectrum to within ~ 3%. The CG results are shown for the two cases in Figs. 8 and 9, respectively. The agreement among the models for these cases can be partially explained by the optical depth of the gas samples. In both cases, the absorptance of the samples in the band center is nearly complete. Thus, a detector cannot see completely through the sample. The degree of temperature variation from s = 0 (~ 400°K) to the point that the detector can see is not as great as the full ~ 400 to ~ 1200°K range of the entire optical path. Apparently, the effective temperature range is small enough to be handled accurately by all of the models. In the band wings, the entire temperature range can be observed, but here the degree of absorption is weak, so that again all of the models yield the same result.

B. NONISOTHERMAL FLAME MEASUREMENTS

The measurements reported by Ludwig et al.[3] were made on a nonisothermal flame composed of four uniform flames in series. The conditions of the individual flame segments for three case studies are shown in Fig. 10, and the experimental radiance spectra in Figs. 11 through 13. A flaw in the experimental spectra is that they are reported with unit W/cm^2-cm^{-1}, and a calibration factor to convert to W/cm^2-sr-cm^{-1} could be found nowhere in Ref. 3 or in supporting documentation of the work. The experimental spectra were scaled by forcing the present CG results to agree with the CG results given with the spectra in Ref. 3.

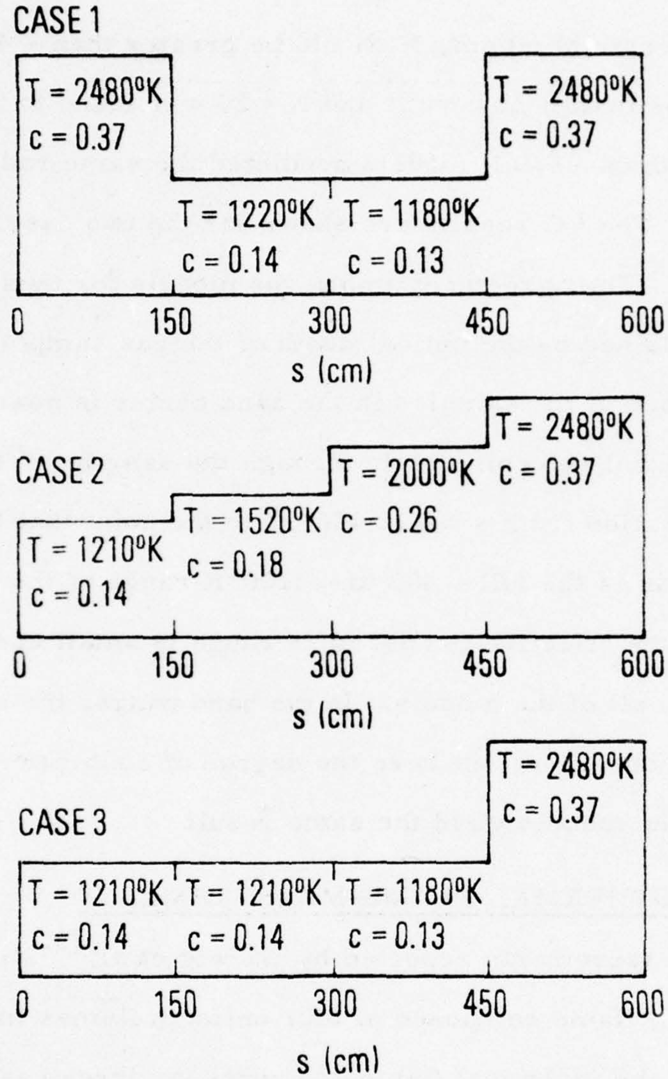

Fig. 10. Temperature and H_2O Concentration Profiles for Nonisothermal Flame Measurements. The pressure for all flame segments and all three cases is p = 1.0 atm, and the foreign broadening gas is O_2.

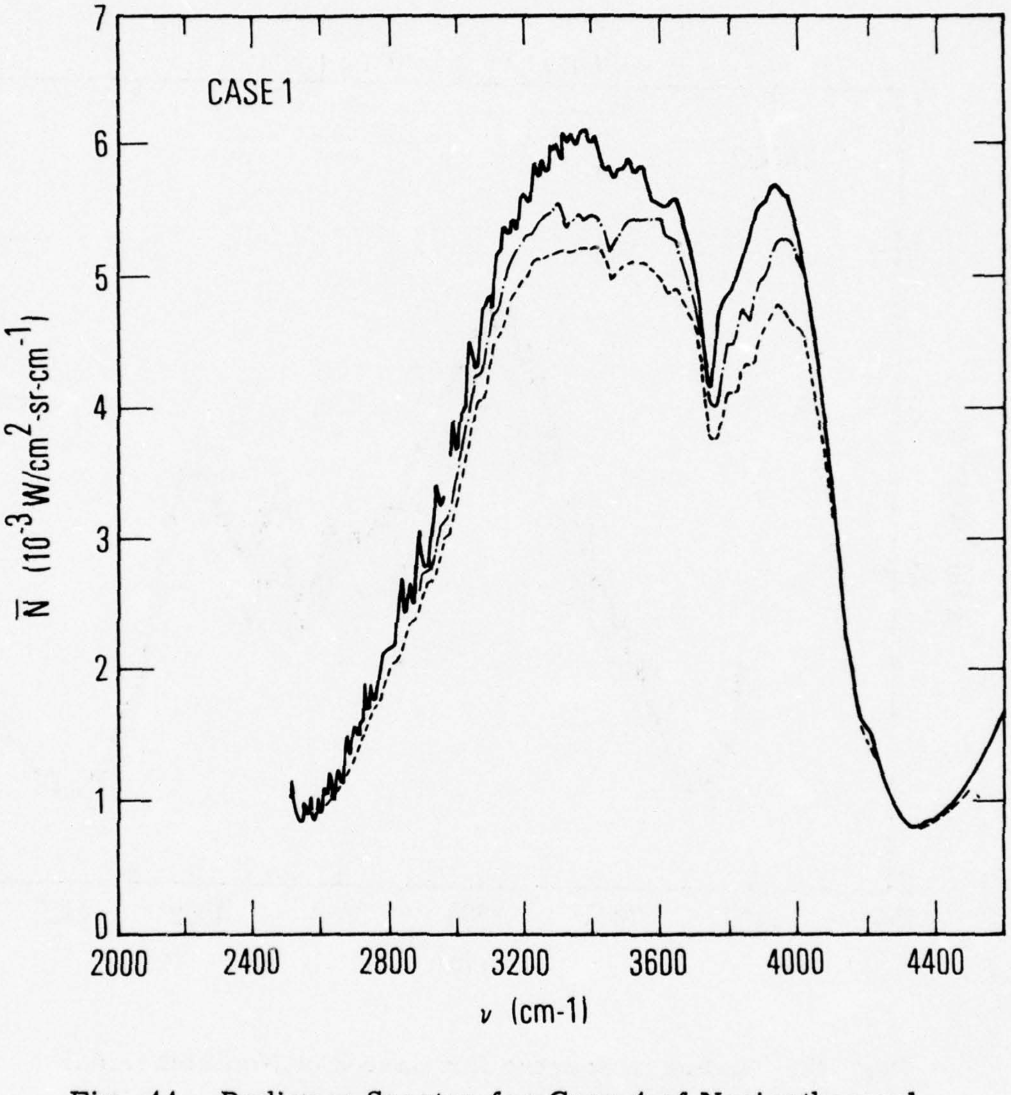

Fig. 11. Radiance Spectra for Case 1 of Nonisothermal Flame Study. ——— experimental, - - - - - - CG approximation, —·—·— derivative approximation.

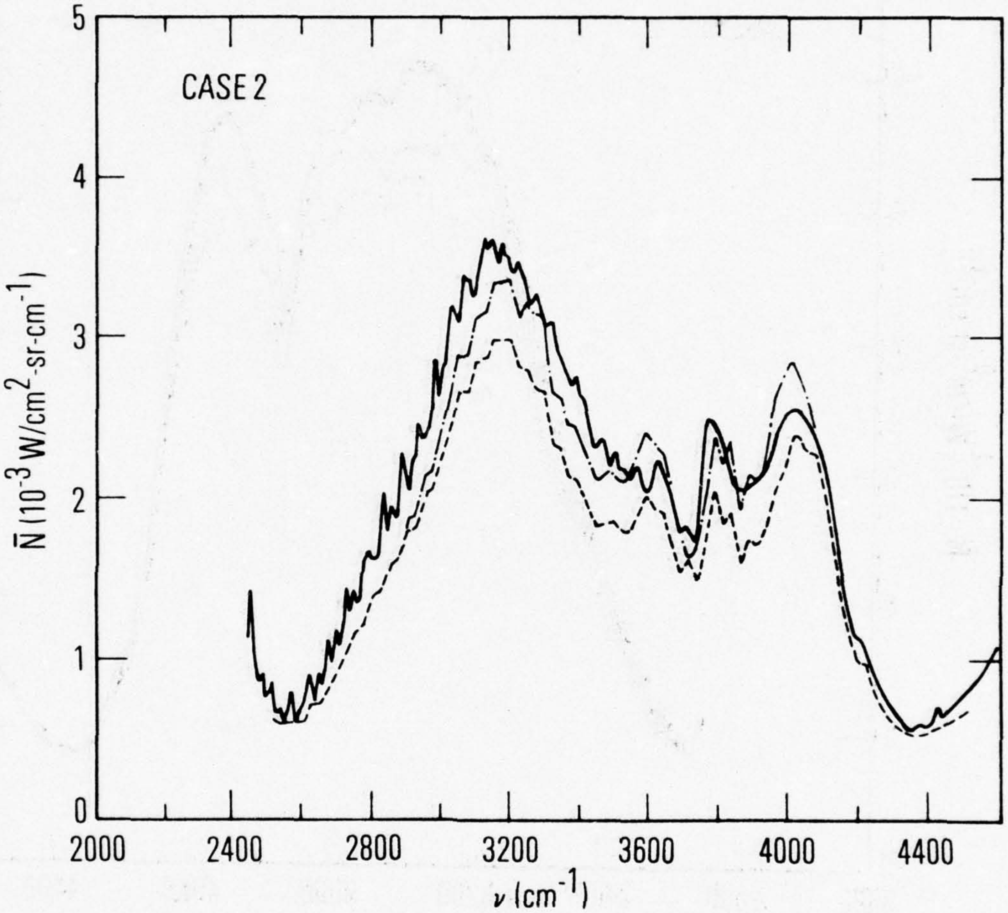

Fig. 12. Radiance Spectra for Case 2 of Nonisothermal Flame Study. ——— experimental, - - - - - - CG approximation, —— · —— · —— derivative approximation.

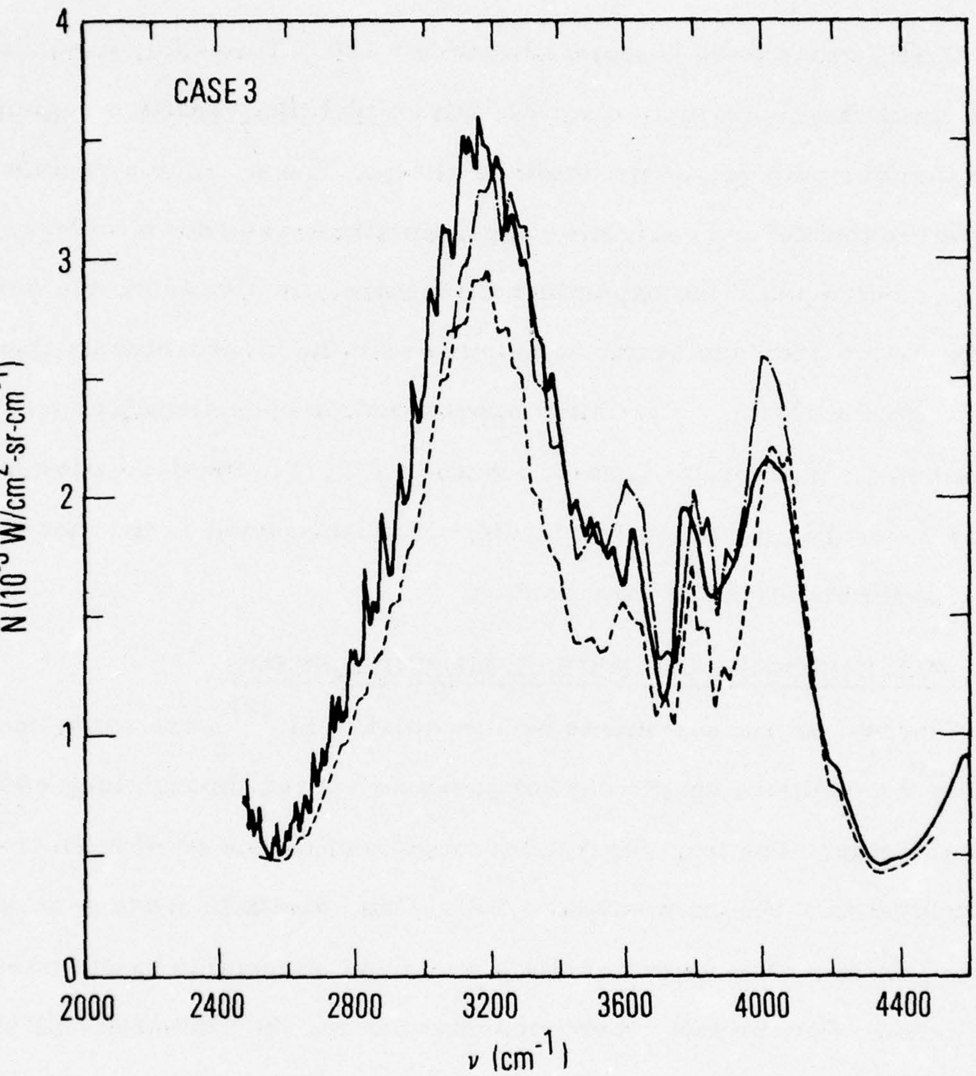

Fig. 13. Radiance Spectra for Case 3 of Nonisothermal Flame Study. ———— experimental, – – – – – – CG approximation, —— · —— · —— · derivative approximation.

Calculations were performed with N = 120. This value was chosen not so much for numerical accuracy, but so that the transition region between the four path segments would be sharp. The predicted radiance spectra for the CG and derivative approximations are shown in Figs. 11 through 13 along with the experimental spectra. In all cases, the derivative approximation provides better agreement with the measurements than does the CG approximation. The latter approximation consistently underpredicts the radiance. Except for Case 1, shown in Fig. 11, the derivative approximation generally increases the predicted radiance level to the measured value, particularly in the band center.

C. HOT-THROUGH-COLD CELL MEASUREMENTS

The recent measurements by Lindquist et al.[7] were made specifically to study the radiance spectra of hot gases as viewed through long cool absorption paths. The experimental arrangement consisted of a 60-cm hot-gas cell coupled to a 100-m absorption cell. Gas conditions were generally set to simulate radiation from missile plumes and absorption by atmospheric slant paths. For the two cases considered here, the emission cell was uniform with $p = 0.10$ atm, $c = 0.50$, and $T = 1200°K$. The absorption cell was uniform with $p = 0.070$ atm, $T = 297°K$, and $c = 0.0143$ (Case 1), $c = 0.143$ (Case 2). In both cells, the foreign gas broadener was N_2. Measurements and predictions of the absorption cell transmittance are shown in Fig. 14. The measured and predicted radiance spectra for the emission cell by itself are shown as the upper curves in Fig. 15(a). Radiance spectra

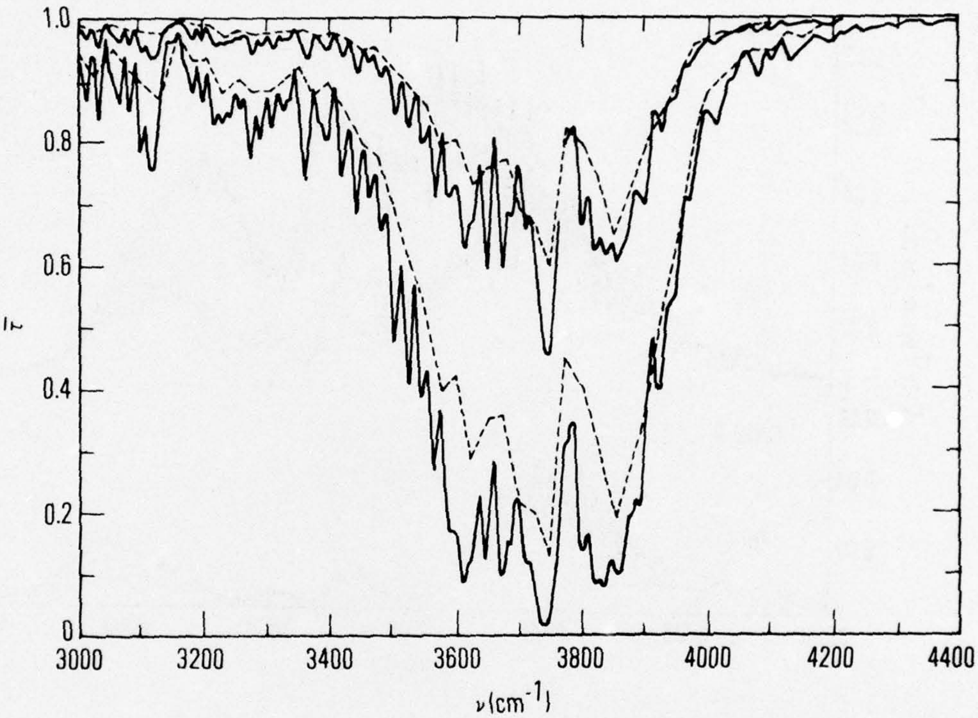

Fig. 14. Absorption Cell Transmittance for Hot-Through-Cold Study. ——— experimental; - - - - - - uniform band model prediction. Upper curves for Case 1 (Run 9R of Ref. 7), lower curves for Case 2 (Run 11MR of Ref. 7).

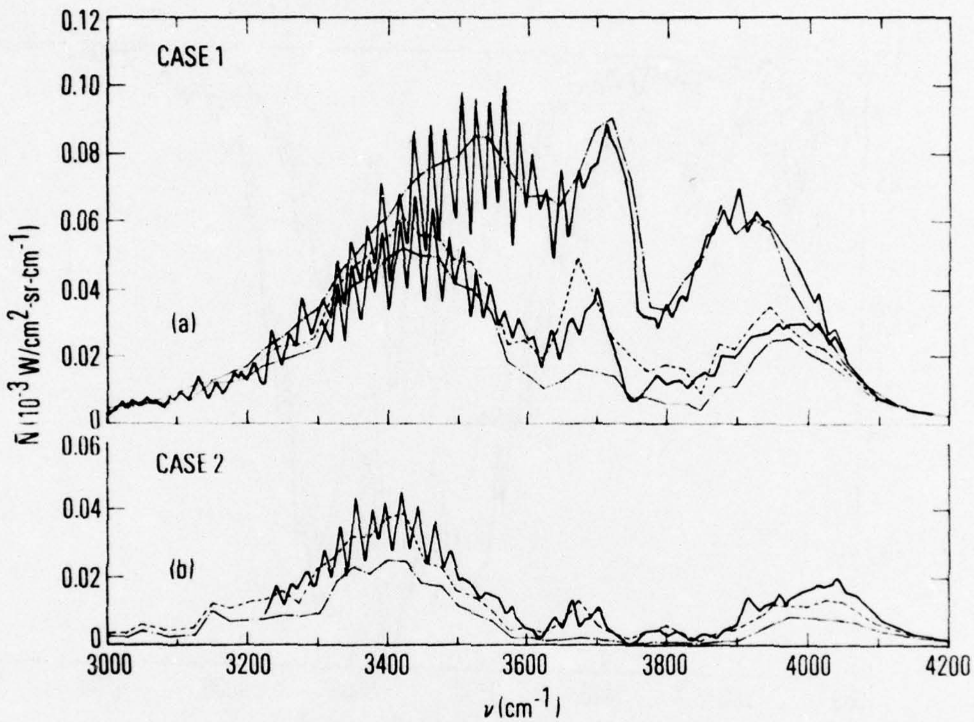

Fig. 15. Radiance Spectra for Hot-Through-Cold Study. ———— experimental; ——·——·—— (upper) uniform band model prediction of hot cell radiance; ——· ——· ——·(lower) transmitted radiance with CG approximation; – – – – – – transmitted radiance with derivative approximation.

as measured through the absorption cell are shown for the two cases in the lower part of Fig. 15(a) and in Fig. 15(b). The spectra computed with the CG and derivative approximations are shown along with the experimental spectra.

Calculations for the absorption-cell transmittance and hot-cell radiance were performed with the uniform path band model. For calculation of path averages in the coupled path arrangement, trapezoidal quadrature was used with the absorption path treated as a single interval and the emission path divided into ten equal size intervals.

For both cases in this study, the CG approximation underpredicts the radiance of the hot source as seen through the absorption path. This effect has been previously noted.[(3)] The results obtained with the derivative approximation are in significantly better agreement with the observed spectra throughout the whole band.

A naive approach to computing the transmitted radiance in the hot-through-cold geometry is to multiply the hot-cell radiance spectrum by the absorption-cell transmittance spectrum. This procedure is valid (in general) only if the emission source is a continuum radiator or if the molecular species of emission and absorption are different. When the two path segments contain common species, line position correlation effects invalidate this approach. The transmitted radiance spectra obtained by this procedure for Case 1 is shown in Fig. 16 along with band-model calculation obtained with the derivative approximation. The enhanced absorption of the absorption cell caused by line correlation is clearly seen to be significant.

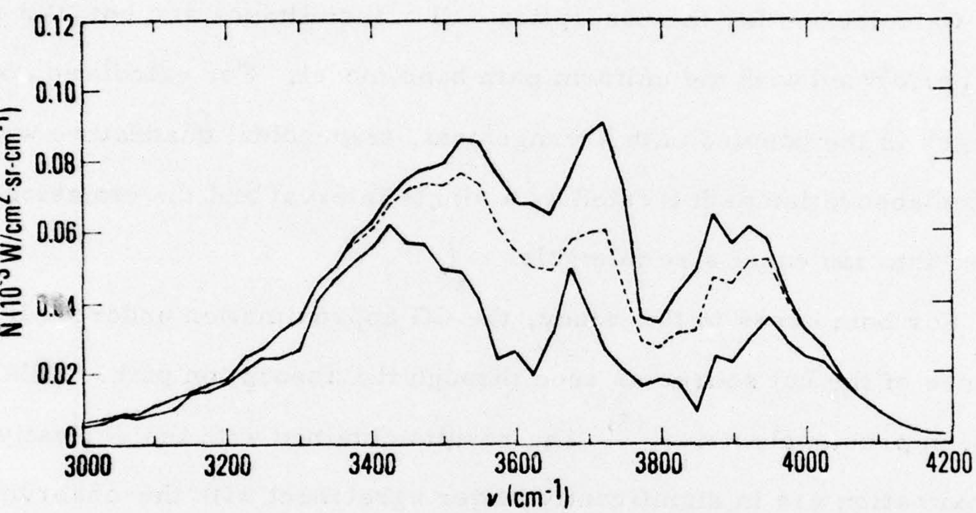

Fig. 16. Band Model Radiance Results (Case 1). ———— (upper) hot-cell radiance; ———— (lower) transmitted radiance with derivative approximation; – – – – – – product of hot-cell radiance and cool-cell transmittance.

APPENDIX

COMBINED H_2O BAND MODEL PARAMETERS LISTING

Tables A-I through A-III are tabulations of the combined band model parameters discussed in Section II. C. The spectral resolution of the parameters is $\sim 25\ cm^{-1}$. The absorption parameter $\overline{k}$ (Table A-I) is given with the natural unit cm^{-1}/atm for the temperatures indicated. The line spacing parameter $\overline{\delta}$ (Table A-II) is represented by its reciprocal, the line density parameter $D = 1/\overline{\delta}$. The nonresonant self-broadening line width parameter $\overline{\gamma}_{H_2O}$ is tabulated in Table A-III. The line width parameter $\overline{\gamma}$ can be obtained from this tabulation through the use of equation (1) and Table I.

Table A-I. Absorption Parameter, $\bar{k}$ (cm^{-1}/atm)

ν(cm^{-1})	100°K	200°K	300°K	500°K	750°K	1000°K	1500°K	2000°K	2500°K	3000°K
2500.	9.160E-09	1.109E-07	6.922E-07	5.952E-06	2.471E-05	1.026E-04	3.058E-04	9.132E-04	1.813E-03	2.257E-03
2525.	3.238E-08	3.548E-07	1.824E-06	7.062E-06	2.656E-05	9.992E-05	3.039E-04	8.886E-04	1.704E-03	2.266E-03
2550.	8.543E-08	9.548E-07	3.400E-06	9.872E-06	3.183E-05	1.026E-04	3.039E-04	8.750E-04	1.660E-03	2.284E-03
2575.	3.458E-07	4.471E-06	1.014E-05	1.962E-05	4.469E-05	1.018E-04	3.058E-04	8.954E-04	1.638E-03	2.302E-03
2600.	2.516E-06	1.624E-05	2.350E-05	3.568E-05	6.012E-05	1.013E-04	3.094E-04	9.186E-04	1.660E-03	2.348E-03
2625.	1.641E-05	3.875E-05	4.231E-05	5.042E-05	7.008E-05	1.048E-04	3.258E-04	1.089E-03	1.955E-03	2.393E-03
2650.	7.411E-05	7.368E-05	6.752E-05	6.150E-05	7.926E-05	1.308E-04	3.658E-04	1.076E-03	1.911E-03	2.457E-03
2675.	1.874E-04	1.106E-04	8.672E-05	7.877E-05	9.695E-05	1.485E-04	4.532E-04	1.290E-03	2.228E-03	2.548E-03
2700.	2.042E-04	9.852E-05	9.191E-05	8.823E-05	1.201E-04	2.078E-04	5.897E-04	1.447E-03	2.523E-03	2.684E-03
2725.	3.322E-04	1.641E-04	1.338E-04	1.270E-04	1.595E-04	2.435E-04	8.026E-04	1.706E-03	2.806E-03	2.894E-03
2750.	3.327E-04	2.429E-04	1.774E-04	1.574E-04	1.864E-04	2.730E-04	9.082E-04	2.007E-03	3.221E-03	3.121E-03
2775.	5.079E-04	2.666E-04	2.375E-04	2.058E-04	2.515E-04	3.958E-04	1.034E-03	2.198E-03	3.342E-03	3.440E-03
2800.	2.065E-04	1.376E-04	1.208E-04	1.879E-04	3.187E-04	5.323E-04	1.372E-03	2.525E-03	3.964E-03	3.795E-03
2825.	1.050E-04	1.017E-04	1.326E-04	2.252E-04	3.948E-04	6.470E-04	1.511E-03	2.798E-03	4.073E-03	4.177E-03
2850.	6.877E-05	4.817E-05	4.901E-05	6.139E-05	1.107E-04	2.705E-04	1.616E-03	3.194E-03	4.707E-03	4.550E-03
2875.	2.187E-05	2.599E-05	3.366E-05	8.059E-05	1.756E-04	3.952E-04	2.002E-03	3.576E-03	4.925E-03	5.005E-03
2900.	1.344E-05	3.181E-05	6.802E-05	2.349E-04	4.442E-04	7.677E-04	2.293E-03	3.986E-03	5.788E-03	5.478E-03
2925.	1.505E-05	8.662E-05	1.798E-04	3.962E-04	6.984E-04	1.231E-03	2.548E-03	4.177E-03	5.853E-03	6.051E-03
2950.	2.579E-06	5.260E-05	2.178E-04	5.894E-04	9.518E-04	1.537E-03	2.894E-03	4.873E-03	6.869E-03	6.688E-03
2975.	6.456E-05	4.081E-04	7.578E-04	1.076E-03	1.419E-03	1.872E-03	3.258E-03	5.255E-03	7.273E-03	7.289E-03
3000.	2.526E-04	1.205E-03	1.744E-03	1.886E-03	1.900E-03	1.914E-03	3.695E-03	6.279E-03	8.539E-03	8.053E-03
3025.	2.354E-03	4.352E-03	4.099E-03	2.834E-03	1.969E-03	2.310E-03	4.0[illegible]4E-03	7.084E-03	9.708E-03	8.827E-03
3050.	2.322E-03	2.587E-03	1.982E-03	1.776E-03	2.094E-03	2.645E-03	5.078E-03	9.036E-03	1.190E-02	9.646E-03
3075.	8.418E-03	6.189E-03	4.037E-03	2.065E-03	2.371E-03	3.030E-03	4.950E-03	9.227E-03	1.190E-02	1.065E-02
3100.	1.559E-02	7.569E-03	4.530E-03	2.320E-03	2.672E-03	3.740E-03	6.770E-03	1.179E-02	1.452E-02	1.174E-02
3125.	2.777E-02	1.073E-02	6.103E-03	3.302E-03	3.822E-03	4.423E-03	8.572E-03	1.365E-02	1.551E-02	1.292E-02
3150.	4.660E-04	3.496E-04	2.809E-04	5.540E-04	1.761E-03	5.596E-03	9.646E-03	1.665E-02	1.835E-02	1.410E-02
3175.	2.540E-02	5.980E-03	2.520E-03	2.346E-03	3.832E-03	6.743E-03	1.152E-02	1.843E-02	1.933E-02	1.547E-02
3200.	2.071E-02	6.740E-03	3.159E-03	3.176E-03	4.440E-03	7.726E-03	1.401E-02	2.088E-02	2.020E-02	1.702E-02
3225.	3.604E-02	1.237E-02	6.403E-03	3.647E-03	5.617E-03	1.026E-02	1.663E-02	2.266E-02	2.250E-02	1.838E-02
3250.	1.282E-02	8.519E-03	5.187E-03	4.507E-03	7.070E-03	1.403E-02	2.129E-02	2.648E-02	2.490E-02	2.002E-02
3275.	2.013E-02	7.995E-03	5.455E-03	5.248E-03	8.959E-03	1.813E-02	2.675E-02	3.003E-02	2.774E-02	2.193E-02
3300.	7.381E-03	6.462E-03	5.418E-03	5.895E-03	1.121E-02	2.277E-02	3.112E-02	3.235E-02	2.872E-02	2.384E-02
3325.	5.480E-03	3.204E-03	3.689E-03	6.693E-03	1.441E-02	2.812E-02	3.658E-02	3.658E-02	3.090E-02	2.548E-02
3350.	4.922E-04	1.089E-03	2.534E-03	7.526E-03	1.919E-02	3.685E-02	4.368E-02	4.027E-02	3.221E-02	2.666E-02
3375.	1.025E-02	6.627E-03	5.637E-03	1.030E-02	2.519E-02	4.614E-02	4.950E-02	4.259E-02	3.287E-02	2.748E-02
3400.	1.112E-03	2.544E-03	4.660E-03	1.412E-02	3.400E-02	5.842E-02	5.624E-02	4.491E-02	3.352E-02	2.803E-02
3425.	7.512E-04	3.881E-03	7.157E-03	2.063E-02	4.611E-02	7.289E-02	6.243E-02	4.532E-02	3.429E-02	2.730E-02
3450.	2.223E-03	8.048E-03	1.310E-02	3.336E-02	6.506E-02	9.091E-02	6.770E-02	4.696E-02	3.309E-02	2.639E-02
3475.	2.337E-03	8.764E-03	1.517E-02	4.547E-02	8.599E-02	9.964E-02	7.007E-02	4.818E-02	3.276E-02	2.475E-02
3500.	6.127E-03	1.783E-02	3.311E-02	7.961E-02	1.182E-01	1.196E-01	7.153E-02	4.300E-02	3.145E-02	2.411E-02

Table A-I. Absorption Parameter, $\bar{k}$ (cm^{-1}/atm) (Continued)

$\nu(cm^{-1})$	100°K	200°K	300°K	500°K	750°K	1000°K	1500°K	2000°K	2500°K	3000°K
3525.	1.280E-02	3.368E-02	5.639E-02	1.179E-01	1.581E-01	1.392E-01	7.444E-02	4.013E-02	2.959E-02	2.193E-02
3550.	1.920E-02	4.055E-02	7.592E-02	1.393E-01	1.635E-01	1.362E-01	7.098E-02	3.836E-02	2.806E-02	2.020E-02
3575.	6.586E-02	1.202E-01	1.943E-01	2.244E-01	1.721E-01	1.209E-01	6.206E-02	3.467E-02	2.512E-02	1.893E-02
3600.	1.095E-01	1.781E-01	2.458E-01	2.273E-01	1.563E-01	1.083E-01	5.205E-02	3.344E-02	2.391E-02	1.829E-02
3625.	2.137E-01	5.057E-01	5.202E-01	3.472E-01	1.963E-01	1.192E-01	5.078E-02	3.180E-02	2.359E-02	1.911E-02
3650.	4.194E-01	6.057E-01	4.710E-01	2.520E-01	1.436E-01	9.473E-02	5.114E-02	3.249E-02	2.391E-02	1.938E-02
3675.	1.350E+00	9.697E-01	5.169E-01	2.995E-01	1.767E-01	1.155E-01	5.733E-02	3.317E-02	2.381E-02	1.820E-02
3700.	3.293E+00	1.249E+00	6.108E-01	2.596E-01	1.613E-01	1.208E-01	6.928E-02	3.824E-02	2.107E-02	1.365E-02
3725.	1.715E+00	6.717E-01	5.530E-01	4.365E-01	2.703E-01	1.545E-01	5.824E-02	2.648E-02	1.343E-02	1.028E-02
3750.	4.425E+00	1.948E+00	1.087E+00	4.585E-01	2.077E-01	1.104E-01	3.926E-02	1.693E-02	1.168E-02	9.828E-03
3775.	1.334E+00	4.042E-01	2.033E-01	8.604E-02	4.358E-02	3.276E-02	2.166E-02	1.570E-02	1.256E-02	9.919E-03
3800.	4.891E+00	1.131E+00	4.622E-01	1.491E-01	6.214E-02	3.368E-02	2.348E-02	1.679E-02	1.223E-02	1.110E-02
3825.	3.722E+00	1.345E+00	6.293E-01	2.206E-01	9.462E-02	5.199E-02	2.803E-02	1.761E-02	1.387E-02	1.238E-02
3850.	2.429E+00	1.693E+00	1.019E+00	4.159E-01	1.659E-01	7.562E-02	3.349E-02	2.198E-02	1.583E-02	1.401E-02
3875.	4.072E-01	6.939E-01	5.958E-01	3.493E-01	1.906E-01	1.151E-01	4.943E-02	2.689E-02	1.824E-02	1.611E-02
3900.	9.023E-02	3.188E-01	3.851E-01	3.005E-01	1.693E-01	1.035E-01	5.023E-02	3.099E-02	2.097E-02	1.793E-02
3925.	4.263E-02	8.210E-02	1.520E-01	1.870E-01	1.488E-01	1.155E-01	5.733E-02	3.317E-02	2.206E-02	1.902E-02
3950.	1.964E-02	2.850E-02	6.991E-02	1.285E-01	1.295E-01	1.058E-01	6.059E-02	3.307E-02	2.206E-02	1.884E-02
3975.	6.518E-03	7.067E-03	1.346E-02	3.853E-02	5.387E-02	7.344E-02	4.277E-02	2.662E-02	2.097E-02	1.729E-02
4000.	8.613E-04	3.094E-03	7.191E-03	2.644E-02	4.460E-02	5.078E-02	3.258E-02	2.170E-02	1.835E-02	1.465E-02
4025.	5.493E-03	6.086E-03	4.851E-03	1.027E-02	2.335E-02	3.001E-02	2.614E-02	1.956E-02	1.463E-02	1.201E-02
4050.	1.159E-03	2.874E-03	3.617E-03	5.727E-03	9.069E-03	1.807E-02	1.613E-02	1.406E-02	1.158E-02	9.464E-03
4075.	2.389E-04	9.064E-04	1.226E-03	2.234E-03	4.731E-03	1.002E-02	1.081E-02	1.093E-02	9.599E-03	7.826E-03
4100.	2.258E-04	1.300E-03	1.877E-03	3.063E-03	4.524E-03	5.760E-03	7.189E-03	6.866E-03	6.661E-03	6.461E-03
4125.	5.190E-05	2.227E-04	4.407E-04	1.353E-03	2.668E-03	3.249E-03	4.477E-03	4.832E-03	5.242E-03	5.442E-03
4150.	4.488E-05	3.074E-04	5.927E-04	1.178E-03	1.805E-03	2.072E-03	3.021E-03	3.522E-03	4.040E-03	4.541E-03
4175.	4.164E-05	1.165E-04	2.425E-04	5.519E-04	9.594E-04	1.215E-03	1.820E-03	2.443E-03	2.927E-03	3.804E-03
4200.	1.899E-05	7.630E-05	2.019E-04	3.616E-04	5.912E-04	9.664E-04	1.494E-03	1.938E-03	2.315E-03	3.167E-03
4225.	1.129E-05	2.579E-05	7.207E-05	1.688E-04	3.104E-04	5.706E-04	1.070E-03	1.529E-03	1.878E-03	2.612E-03
4250.	3.310E-06	1.577E-05	5.487E-05	1.454E-04	2.739E-04	5.160E-04	9.318E-04	1.379E-03	1.791E-03	2.148E-03
4275.	1.698E-06	9.891E-06	2.818E-05	7.591E-05	1.798E-04	4.259E-04	6.661E-04	1.108E-03	1.485E-03	1.720E-03
4300.	3.801E-07	2.659E-06	1.433E-05	5.827E-05	1.487E-04	3.795E-04	5.569E-04	9.023E-04	1.256E-03	1.365E-03
4325.	4.733E-07	1.420E-06	4.323E-06	2.400E-05	8.490E-05	3.003E-04	4.950E-04	8.013E-04	1.136E-03	1.147E-03
4350.	2.389E-07	9.526E-07	3.575E-06	1.459E-05	6.209E-05	2.643E-04	4.040E-04	6.784E-04	1.006E-03	1.083E-03
4375.	5.821E-08	4.6[illegible]0E-07	2.058E-06	9.123E-06	4.305E-05	2.031E-04	3.786E-04	6.361E-04	9.566E-04	1.083E-03
4400.	3.299E-08	2.009E-07	1.072E-06	6.409E-06	3.341E-05	1.742E-04	3.367E-04	6.347E-04	9.981E-04	1.119E-03
4425.	9.967E-08	3.426E-07	1.148E-06	5.012E-06	2.613E-05	1.362E-04	3.167E-04	6.211E-04	1.021E-03	1.165E-03
4450.	9.209E-08	5.557E-07	1.635E-06	6.240E-06	2.874E-05	1.324E-04	3.312E-04	6.224E-04	1.060E-03	1.219E-03
4475.	9.999E-09	5.401E-07	2.413E-06	7.390E-06	2.611E-05	9.227E-05	2.439E-04	6.279E-04	1.136E-03	1.292E-03
4500.	2.515E-07	2.101E-06	6.394E-06	2.021E-05	5.067E-05	8.982E-05	2.803E-04	6.511E-04	1.223E-03	1.374E-03

Table A-II. Line Density Parameter, $1/\bar{\delta}$ (lines/cm^{-1})

ν(cm^{-1})	100°K	200°K	300°K	500°K	750°K	1000°K	1500°K	2000°K	2500°K	3000°K
2500.	7.087E-01	1.637E+00	1.817E+00	2.238E+00	2.905E+00	3.770E+00	6.350E+00	1.380E+01	6.070E+01	2.510E+02
2525.	9.808E-01	1.991E+00	2.190E+00	2.649E+00	3.360E+00	4.263E+00	6.860E+00	1.510E+01	6.680E+01	2.670E+02
2550.	1.115E+00	1.677E+00	1.881E+00	2.365E+00	3.148E+00	4.192E+00	7.430E+00	1.650E+01	7.360E+01	2.840E+02
2575.	1.118E+00	1.299E+00	1.366E+00	1.592E+00	2.300E+00	3.344E+00	7.070E+00	1.580E+01	6.940E+01	2.600E+02
2600.	1.393E+00	1.546E+00	1.764E+00	2.156E+00	2.866E+00	3.809E+00	6.730E+00	1.520E+01	6.540E+01	2.370E+02
2625.	8.762E-01	1.148E+00	1.430E+00	1.924E+00	2.599E+00	3.512E+00	6.410E+00	1.460E+01	6.160E+01	2.170E+02
2650.	1.058E+00	1.398E+00	1.701E+00	2.215E+00	2.853E+00	3.676E+00	6.100E+00	1.400E+01	5.810E+01	1.980E+02
2675.	6.877E-01	1.030E+00	1.417E+00	2.040E+00	2.649E+00	3.440E+00	5.800E+00	1.350E+01	5.470E+01	1.810E+02
2700.	8.007E-01	1.649E+00	2.756E+00	4.061E+00	4.387E+00	4.739E+00	5.530E+00	1.290E+01	5.160E+01	1.650E+02
2725.	1.334E+00	2.302E+00	2.841E+00	3.326E+00	3.730E+00	4.183E+00	5.260E+00	1.240E+01	4.860E+01	1.510E+02
2750.	9.336E-01	1.504E+00	1.990E+00	2.404E+00	2.888E+00	3.470E+00	5.010E+00	1.190E+01	4.580E+01	1.370E+02
2775.	1.053E+00	1.302E+00	1.562E+00	1.973E+00	2.460E+00	3.068E+00	4.770E+00	1.140E+01	4.320E+01	1.250E+02
2800.	1.531E+00	1.766E+00	1.968E+00	2.222E+00	2.657E+00	3.176E+00	4.540E+00	1.100E+01	4.070E+01	1.150E+02
2825.	1.844E+00	2.439E+00	2.616E+00	2.964E+00	3.257E+00	3.578E+00	4.320E+00	1.050E+01	3.830E+01	1.050E+02
2850.	1.714E+00	3.075E+00	3.494E+00	3.862E+00	4.533E+00	5.321E+00	7.331E+00	1.010E+01	3.610E+01	9.600E+01
2875.	1.576E+00	2.484E+00	3.113E+00	3.551E+00	4.203E+00	4.976E+00	6.972E+00	9.770E+00	3.410E+01	8.760E+01
2900.	2.011E+00	2.124E+00	2.234E+00	2.432E+00	2.705E+00	3.008E+00	3.720E+00	9.380E+00	3.210E+01	8.000E+01
2925.	8.209E-01	9.863E-01	1.258E+00	1.689E+00	2.032E+00	2.445E+00	3.540E+00	9.010E+00	3.020E+01	7.300E+01
2950.	1.100E+00	1.200E+00	1.282E+00	1.570E+00	1.900E+00	[illegible]	3.370E+00	8.650E+00	2.850E+01	6.670E+01
2975.	4.437E-01	7.631E-01	9.984E-01	1.470E+00	1.866E+00	2.236E+00	3.210E+00	8.310E+00	2.680E+01	6.090E+01
3000.	4.412E-01	8.017E-01	1.032E+00	1.433E+00	[illegible]	2.149E+00	3.060E+00	7.980E+00	2.530E+01	5.560E+01
3025.	4.539E-01	6.573E-01	8.273E-01	1.346E+00	[illegible]	2.221E+00	2.910E+00	7.660E+00	2.390E+01	5.080E+01
3050.	3.117E-01	3.988E-01	5.304E-01	1.031E+00	[illegible]	2.018E+00	2.770E+00	7.360E+00	2.250E+01	4.640E+01
3075.	3.717E-01	5.279E-01	6.603E-01	9.897E-01	[illegible]	1.647E+00	2.640E+00	7.070E+00	2.120E+01	4.240E+01
3100.	3.948E-01	7.276E-01	1.003E+00	1.533E+00	2.007E+00	2.162E+00	2.510E+00	6.790E+00	2.000E+01	3.870E+01
3125.	4.362E-01	6.979E-01	1.041E+00	1.857E+00	2.382E+00	2.385E+00	2.390E+00	6.520E+00	1.880E+01	3.530E+01
3150.	1.008E-01	2.376E-01	7.774E-01	1.738E+00	1.834E+00	1.969E+00	2.270E+00	6.260E+00	1.770E+01	3.230E+01
3175.	2.595E-01	4.005E-01	6.999E-01	1.824E+00	2.242E+00	2.218E+00	2.170E+00	6.010E+00	1.670E+01	2.950E+01
3200.	2.759E-01	3.350E-01	4.966E-01	1.140E+00	1.353E+00	1.557E+00	2.060E+00	5.770E+00	1.570E+01	2.690E+01
3225.	4.484E-01	6.712E-01	9.974E-01	1.894E+00	2.291E+00	2.734E+00	3.891E+00	5.540E+00	1.480E+01	2.460E+01
3250.	3.177E-01	4.341E-01	6.194E-01	1.151E+00	1.553E+00	1.679E+00	2.030E+00	4.690E+00	1.090E+01	2.660E+01
3275.	2.750E-01	6.905E-01	1.179E+00	1.880E+00	1.914E+00	1.949E+00	2.020E+00	4.490E+00	9.580E+00	2.290E+01
3300.	4.490E-01	8.551E-01	1.200E+00	1.812E+00	1.836E+00	1.860E+00	1.910E+00	4.620E+00	9.660E+00	1.730E+01
3325.	1.619E-01	7.547E-01	1.449E+00	2.371E+00	2.680E+00	2.922E+00	3.474E+00	4.130E+00	8.790E+00	1.700E+01
3350.	2.857E-01	1.120E+00	1.397E+00	1.977E+00	2.223E+00	2.500E+00	3.163E+00	4.000E+00	8.590E+00	1.370E+01
3375.	2.773E-01	7.633E-01	1.486E+00	2.538E+00	2.733E+00	2.944E+00	3.414E+00	3.960E+00	8.410E+00	1.360E+01
3400.	3.714E-01	9.080E-01	1.299E+00	1.953E+00	2.186E+00	2.447E+00	3.065E+00	3.840E+00	8.170E+00	1.240E+01
3425.	4.503E-01	8.549E-01	1.317E+00	1.975E+00	2.219E+00	2.493E+00	3.146E+00	3.970E+00	7.610E+00	1.070E+01
3450.	5.242E-01	1.063E+00	1.732E+00	2.136E+00	2.285E+00	2.444E+00	2.797E+00	3.200E+00	6.290E+00	9.580E+00
3475.	5.643E-01	1.081E+00	1.649E+00	1.833E+00	2.009E+00	2.203E+00	2.647E+00	3.180E+00	6.430E+00	1.010E+01
3500.	3.757E-01	9.937E-01	1.400E+00	1.498E+00	1.574E+00	1.650E+00	2.477E+00	3.720E+00	6.850E+00	1.030E+01

Table A-II. Line Density Parameter, $1/\bar{\delta}$ (lines /cm^{-1}) (Continued)

ν(cm^{-1})	100°K	200°K	300°K	500°K	750°K	1000°K	1500°K	2000°K	2500°K	3000°K
3525.	4.494E-01	1.042E+00	1.410E+00	1.518E+00	1.626E+00	1.718E+00	2.638E+00	4.050E+00	7.790E+00	1.320E+01
3550.	6.459E-01	1.407E+00	1.463E+00	1.445E+00	1.574E+00	1.688E+00	2.618E+00	4.060E+00	8.090E+00	1.590E+01
3575.	7.438E-01	1.396E+00	1.306E+00	1.273E+00	1.366E+00	1.455E+00	2.484E+00	4.240E+00	8.940E+00	1.850E+01
3600.	5.399E-01	8.967E-01	8.828E-01	1.019E+00	1.235E+00	1.396E+00	2.000E+00	4.400E+00	8.420E+00	1.400E+01
3625.	7.000E-01	7.500E-01	7.768E-01	8.628E-01	1.032E+00	1.188E+00	1.890E+00	4.210E+00	7.170E+00	9.410E+00
3650.	5.933E-01	5.966E-01	6.390E-01	8.188E-01	1.139E+00	1.412E+00	2.353E+00	3.920E+00	7.090E+00	1.000E+01
3675.	4.908E-01	5.031E-01	5.766E-01	9.139E-01	1.470E+00	1.820E+00	2.708E+00	4.030E+00	6.690E+00	8.770E+00
3700.	5.830E-01	7.193E-01	9.728E-01	1.734E+00	2.411E+00	2.649E+00	3.010E+00	3.420E+00	7.420E+00	1.290E+01
3725.	3.163E-01	9.228E-01	1.259E+00	1.553E+00	1.759E+00	2.086E+00	2.935E+00	4.130E+00	1.570E+01	4.470E+01
3750.	5.789E-01	8.017E-01	9.275E-01	1.149E+00	1.489E+00	1.930E+00	3.260E+00	4.340E+00	9.870E+00	2.010E+01
3775.	3.388E-01	5.933E-01	8.572E-01	1.396E+00	1.919E+00	2.238E+00	2.746E+00	3.370E+00	6.520E+00	1.580E+01
3800.	2.756E-01	3.943E-01	5.332E-01	9.046E-01	1.413E+00	1.814E+00	2.809E+00	4.350E+00	1.220E+01	2.450E+01
3825.	4.696E-01	5.710E-01	6.787E-01	9.914E-01	1.418E+00	1.736E+00	2.789E+00	4.480E+00	9.020E+00	1.360E+01
3850.	4.976E-01	6.863E-01	8.089E-01	1.041E+00	1.319E+00	1.538E+00	1.880E+00	3.870E+00	8.240E+00	1.260E+01
3875.	6.049E-01	7.629E-01	8.935E-01	1.203E+00	1.603E+00	1.917E+00	2.579E+00	3.470E+00	7.300E+00	1.160E+01
3900.	5.971E-01	7.375E-01	8.225E-01	1.033E+00	1.306E+00	1.522E+00	2.341E+00	3.600E+00	6.790E+00	8.890E+00
3925.	3.222E-01	9.549E-01	1.029E+00	1.197E+00	1.444E+00	1.641E+00	2.431E+00	3.600E+00	7.100E+00	9.300E+00
3950.	2.298E-01	8.712E-01	9.924E-01	1.122E+00	1.317E+00	1.472E+00	2.436E+00	4.030E+00	7.910E+00	1.080E+01
3975.	2.916E-01	7.833E-01	1.128E+00	1.214E+00	1.330E+00	1.457E+00	1.750E+00	4.510E+00	7.630E+00	9.940E+00
4000.	2.505E-01	5.223E-01	8.927E-01	9.401E-01	9.527E-01	9.766E-01	1.790E+00	4.840E+00	8.040E+00	1.160E+01
4025.	2.985E-01	4.046E-01	7.915E-01	1.196E+00	1.308E+00	1.430E+00	1.710E+00	5.690E+00	1.180E+01	1.790E+01
4050.	3.307E-01	4.201E-01	6.071E-01	1.171E+00	1.347E+00	1.549E+00	2.050E+00	5.850E+00	1.440E+01	2.950E+01
4075.	5.000E-01	5.566E-01	6.149E-01	9.395E-01	1.132E+00	1.364E+00	1.980E+00	5.160E+00	1.220E+01	2.770E+01
4100.	4.000E-01	4.042E-01	4.163E-01	5.425E-01	6.819E-01	1.008E+00	2.200E+00	8.850E+00	2.280E+01	4.040E+01
4125.	5.000E-01	5.000E-01	5.000E-01	5.685E-01	7.118E-01	1.078E+00	2.470E+00	1.320E+01	2.490E+01	2.860E+01
4150.	7.000E-01	7.000E-01	7.000E-01	7.587E-01	8.416E-01	1.249E+00	2.750E+00	1.620E+01	3.280E+01	6.910E+01
4175.	5.000E-01	5.000E-01	5.000E-01	5.111E-01	5.368E-01	9.589E-01	3.060E+00	1.790E+01	3.760E+01	7.940E+01
4200.	7.500E-01	7.500E-01	7.500E-01	7.583E-01	7.758E-01	1.270E+00	3.400E+00	1.980E+01	4.300E+01	9.120E+01
4225.	1.100E+00	1.100E+00	1.118E+00	1.370E+00	1.765E+00	2.275E+00	3.780E+00	2.190E+01	4.920E+01	1.040E+02
4250.	1.200E+00	1.200E+00	1.192E+00	1.471E+00	1.913E+00	2.489E+00	4.210E+00	2.420E+01	5.630E+01	1.200E+02
4275.	1.000E+00	1.000E+00	1.046E+00	1.343E+00	1.835E+00	2.507E+00	4.680E+00	2.670E+01	6.440E+01	1.380E+02
4300.	1.100E+00	1.100E+00	1.160E+00	1.490E+00	2.038E+00	2.786E+00	5.210E+00	2.950E+01	7.370E+01	1.590E+02
4325.	1.104E+00	1.662E+00	1.868E+00	2.256E+00	2.857E+00	3.618E+00	5.800E+00	3.260E+01	8.430E+01	1.820E+02
4350.	1.000E+00	1.000E+00	1.013E+00	1.026E+00	1.043E+00	1.060E+00	6.450E+00	3.600E+01	9.640E+01	2.090E+02
4375.	8.000E-01	8.000E-01	8.442E-01	1.107E+00	1.553E+00	2.180E+00	7.170E+00	3.990E+01	1.100E+02	2.410E+02
4400.	7.500E-01	7.500E-01	7.874E-01	9.224E-01	1.124E+00	1.370E+00	7.980E+00	4.400E+01	1.260E+02	2.770E+02
4425.	6.399E-01	7.500E-01	8.357E-01	9.311E-01	1.066E+00	1.220E+00	6.930E+00	3.940E+01	1.120E+02	2.510E+02
4450.	3.018E-01	5.014E-01	5.519E-01	6.686E-01	8.497E-01	1.080E+00	6.010E+00	3.520E+01	9.940E+01	2.280E+02
4475.	2.400E-01	2.400E-01	2.521E-01	3.691E-01	5.943E-01	9.570E-01	5.220E+00	3.140E+01	8.820E+01	2.070E+02
4500.	1.805E-01	4.201E-01	4.400E-01	4.710E-01	6.316E-01	8.470E-01	4.520E+00	2.810E+01	7.830E+01	1.890E+02

Table A-III. Nonresonant Self-Broadening Line Width Parameter

ν (cm^{-1})	$\bar{\gamma}_{H_2O}$ (cm^{-1}/atm)	ν (cm^{-1})	$\bar{\gamma}_{H_2O}$ (cm^{-1}/atm)
2500.	5.921E-02	3525.	7.634E-02
2525.	5.842E-02	3550.	7.986E-02
2550.	6.038E-02	3575.	8.201E-02
2575.	6.622E-02	3600.	8.514E-02
2600.	6.412E-02	3625.	8.761E-02
2625.	6.672E-02	3650.	8.620E-02
2650.	7.735E-02	3675.	8.117E-02
2675.	7.865E-02	3700.	8.714E-02
2700.	7.678E-02	3725.	9.002E-02
2725.	8.453E-02	3750.	9.073E-02
2750.	8.499E-02	3775.	8.318E-02
2775.	8.397E-02	3800.	7.786E-02
2800.	8.238E-02	3825.	7.722E-02
2825.	7.479E-02	3850.	7.942E-02
2850.	7.176E-02	3875.	7.181E-02
2875.	6.605E-02	3900.	6.893E-02
2900.	6.567E-02	3925.	6.712E-02
2925.	6.248E-02	3950.	6.759E-02
2950.	6.753E-02	3975.	6.466E-02
2975.	6.379E-02	4000.	6.741E-02
3000.	6.958E-02	4025.	7.484E-02
3025.	7.808E-02	4050.	7.177E-02
3050.	7.682E-02	4075.	7.952E-02
3075.	7.621E-02	4100.	8.564E-02
3100.	8.023E-02	4125.	8.931E-02
3125.	8.044E-02	4150.	8.333E-02
3150.	7.384E-02	4175.	8.393E-02
3175.	7.644E-02	4200.	8.069E-02
3200.	7.752E-02	4225.	7.615E-02
3225.	7.660E-02	4250.	6.623E-02
3250.	7.892E-02	4275.	6.943E-02
3275.	7.526E-02	4300.	6.602E-02
3300.	7.015E-02	4325.	6.434E-02
3325.	6.602E-02	4350.	7.183E-02
3350.	6.609E-02	4375.	6.782E-02
3375.	6.435E-02	4400.	7.368E-02
3400.	6.495E-02	4425.	7.515E-02
3425.	6.610E-02	4450.	7.171E-02
3450.	6.764E-02	4475.	7.020E-02
3475.	7.182E-02	4500.	7.208E-02
3500.	7.608E-02		

REFERENCES

1. B. Krakow, H. J. Babrov, G. J. Maclay, and A. Shabott, "Use of the Curtis-Godson Approximation in Calculations of Radiant Heating by Inhomogeneous Hot Gases," Applied Optics 5, 1791-1800 (1966).
2. Study on Exhaust Plumes Radiation Predictions: Final Report, GDC-DBE66-017, General Dynamics/Convair, San Diego, California (December 1966).
3. C. B. Ludwig, W. Malkmus, J. E. Reardon, and J. A. L. Thompson, Handbook of Infrared Radiation from Combustion Gases, ed. R. Goulard and J. A. L. Thompson, NASA SP-3080, Marshall Space Flight Center, Huntsville, Alabama (1973).
4. F. S. Simmons, "Band Models for Nonisothermal Radiating Gases," Applied Optics 5, 1801-1811 (1966).
5. F. S. Simmons, H. Y. Yamada, and C. B. Arnold, Measurement of Temperature Profiles in Hot Gases by Emission-Absorption Spectroscopy, NASA CR-72491, Lewis Research Center, Cleveland, Ohio (April 1969).
6. F. S. Simmons, C. B. Arnold, and G. H. Lindquist, Measurement of Temperature Profiles in Flames by Emission-Absorption Spectroscopy, NASA CR-120894, Lewis Research Center, Cleveland, Ohio (February 1972).

7. G. H. Lindquist, C. B. Arnold, and R. L. Spellicy, Atmospheric Absorption Applied to Plume Emission: Experimental and Analytical Investigations of Hot Gas Emission Attenuated by Cold Gases, ERIM 102700-20-F, Environmental Research Institute of Michigan, Ann Arbor, Michigan (August 1975).

8. S. J. Young, Band Model Parameters for the 2.7-μm Bands of H_2O and CO_2 in the 100 to 3000°K Temperature Range, TR-0076(6970)-4, The Aerospace Corporation, El Segundo, California (31 July 1975).

9. R. A. McClatchey, W. S. Benedict, S. A. Clough, D. E. Burch, R. F. Calfe, K. Fox, L. S. Rothman, and J. S. Garing, AFCRL Atmospheric Absorption Line Parameters Compilation, AFCRL-TR-73-0096, Air Force Geophysics Laboratory (formerly Air Force Cambridge Research Laboratory), Hanscomb AFB, Massachusetts (26 January 1973).

10. C. B. Ludwig, "Measurements of the Curves-of-Growth of Hot Water Vapor," Applied Optics 10, 1057-1073 (1971).

11. D. E. Burch, D. A. Gryvnak, and R. R. Patty, Absorption by H_2O between 2800 and 4500 cm^{-1} (2.7 Micron Region), U-3202, Aeronutronic Division, Philco-Ford Corporation, Newport Beach, California (30 September 1965).

12. F. S. Simmons, C. B. Arnold, and D. H. Smith, Studies of Infrared Radiative Transfer in Hot Gases, I: Spectral Absorptance Measurements in the 2.7μ H_2O Bands, Report No. 4613-91-T, Willow Run Laboratory, Ann Arbor, Michigan (August 1965).

13. P. C. Sukanek and L. P. Davis, An Assessment of the NASA Band Model Formulation for Calculating the Radiance and Transmission of Hot and Cool Gases, AFRPL-TR-76-9, Air Force Rocket Propulsion Laboratory, Edwards AFB, California (February 1976).

LABORATORY OPERATIONS

The Laboratory Operations of The Aerospace Corporation is conducting experimental and theoretical investigations necessary for the evaluation and application of scientific advances to new military concepts and systems. Versatility and flexibility have been developed to a high degree by the laboratory personnel in dealing with the many problems encountered in the nation's rapidly developing space and missile systems. Expertise in the latest scientific developments is vital to the accomplishment of tasks related to these problems. The laboratories that contribute to this research are:

Aerophysics Laboratory: Launch and reentry aerodynamics, heat transfer, reentry physics, chemical kinetics, structural mechanics, flight dynamics, atmospheric pollution, and high-power gas lasers.

Chemistry and Physics Laboratory: Atmospheric reactions and atmospheric optics, chemical reactions in polluted atmospheres, chemical reactions of excited species in rocket plumes, chemical thermodynamics, plasma and laser-induced reactions, laser chemistry, propulsion chemistry, space vacuum and radiation effects on materials, lubrication and surface phenomena, photosensitive materials and sensors, high precision laser ranging, and the application of physics and chemistry to problems of law enforcement and biomedicine.

Electronics Research Laboratory: Electromagnetic theory, devices, and propagation phenomena, including plasma electromagnetics; quantum electronics, lasers, and electro-optics; communication sciences, applied electronics, semiconducting, superconducting, and crystal device physics, optical and acoustical imaging; atmospheric pollution; millimeter wave and far-infrared technology.

Materials Sciences Laboratory: Development of new materials; metal matrix composites and new forms of carbon; test and evaluation of graphite and ceramics in reentry; spacecraft materials and electronic components in nuclear weapons environment; application of fracture mechanics to stress corrosion and fatigue-induced fractures in structural metals.

Space Sciences Laboratory: Atmospheric and ionospheric physics, radiation from the atmosphere, density and composition of the atmosphere, aurorae and airglow; magnetospheric physics, cosmic rays, generation and propagation of plasma waves in the magnetosphere; solar physics, studies of solar magnetic fields; space astronomy, x-ray astronomy; the effects of nuclear explosions, magnetic storms, and solar activity on the earth's atmosphere, ionosphere, and magnetosphere; the effects of optical, electromagnetic, and particulate radiations in space on space systems.

THE AEROSPACE CORPORATION
El Segundo, California